International
Journal
Of Advanced Research in Engineering& Management (IJAREM)
ISSN: 2456-2033 || PP. 10-27

High-order electrical equivalent circuit modeling research for an accurate lithium-ion battery state prediction

Md. Amdadul Haque[1], Shunli Wang[1], Carlos Fernandez[2], Chunmei Yu[1], Mingfang He[1], Etse Dablu Bobobee[1]
[1]*School of Information Engineering, Southwest University of Science and Technology, Mianyang 621010, China*
[2]*School of Pharmacy and Life Sciences, Robert Gordon University, Aberdeen AB10-7GJ, UK*

Abstract: For high-power lithium-ion battery packs, battery modeling and iterative state calculation in the battery management system are important, since their accuracy influences their working performance and safety. To realize the iterative computation procedure, and predict the state of charge for optimal performance, as well as providing reliable and timely information on an improved extended Kalman filter system and a battery high-order electrical equivalent circuit model are combined in this paper to dynamically approximate the SOC of a battery. The traditional equivalent circuit model was used alongside the suggested high-order electrical equivalent circuit model in the same algorithm to ensure the model's efficacy. Experiments indicate that the results from using the high-order electrical equivalent circuit model with improved EKF have a strong convergence speed, are more stable, and have a high precision of accuracy in the state of charge estimation, and the estimation accuracy can reach third-order precision. Under extreme voltage and current changes, the maximum state of charge error estimated based on the traditional equivalent circuit model using the improved EKF algorithm was 2.96% representing an accuracy of 97.04%, and the maximum error based on the established high-order electrical model using the improved extended Kalman filtering algorithm was 1.83% representing an accuracy of 98.17%. The estimation error remains at 1.83 percent, which may be reduced by 1.13 percent when compared to the traditional technique. It can give a theoretical safety protection framework for the lithium-ion battery pack's energy management.

Keywords: Lithium-ion batteries; state of charge; parameter detection; high-order modeling; improved extended Kalman filter algorithm;

1. Introduction

A detailed state of charge (SOC) calculation for lithium-ion batteries is intended in this research and allows safe use of it on digital devices like electric vehicles (EVs), hybrid vehicles (HVs), and stationary devices[1]. To use multiple methodologies to offer precise precision. From a global viewpoint, battery management systems (BMS) research[2]covers those that present an entire architecture that adopts a distributed framework to achieve greater scalability and usability[3]. Different approaches to developing a BMS rely on the functionality needed by the particular application, but most of them concentrate on main functions such as SOC estimation and the method of balancing[4]. The development of electric and hybrid electric vehicles is towards the creation of smart BMS in artificial intelligence for the evaluation of the battery state[5, 6]. For large battery packs with applications like EVs and grid convergence, a dynamic and scalable BMS based on models is particularly relevant. Therefore, SOC estimation has captured the interest of many scholars, and many different approaches have been suggested[7, 8]. The combination of the OCV algorithm method, a maximum charge detection system load observer, and the CC approach with an improved extended Kalman filter algorithm (EKF) is the main feature[9]. When certain strategies are used, it is hard to decide the precise strategy. However, two types of direct and indirect methods as well as several subcategories summarizing patterns in the SOC estimate are correctly described and matched based on the distinction rendered in them.

By creating a statistical model, the battery model was used to estimate the interaction between the physical conditions and the internal states of a battery. For the SOC estimation needed, models in a discrete-time state-space type are often used. The use of high-order electrical equivalent circuit models is stated in current literature as being commonly used as a basis for model-based estimation and control[10]. For the simulation of lithium-ion batteries[11], comparable circuit models are usually chosen, including the Rint model[12], the Thevenin model[13], the RC model, and the partnership for a New Generation Vehicle (PNGV)[14]. These models all use the first-order RC, second-order RC, and third-order RC to correctly model the battery. Among

them, the Thevenin model is commonly used but not precise enough because, depending on the nature and state of the battery, all its features will change[15].

To optimize the model recognizable and integrated SOC and parameter estimation[16, 17] as a way of figuring out SOC in the presence of uncertain or time-varying battery parameters[18], work is performed on parameter recognition using the optimal configuration of charging/discharge cycles[19]. These studies either assume an accurate SOC/OCV relationship available or impose approximations such as OCV being piece-wise linear with SOC or constant during discharging[20]. RC parameters are obtained by evaluating the transients in a battery voltage responding under some excitation, such as experiments with constant or pulse currents. In an ECM, the voltage source usually reflects the open-circuit voltage of the battery (OCV)[21], which depending on the SOC. By charging or discharging the battery using a limited current, a connection between SOC and OCV can be established[22]. An analytical approach that reduced the problem of solving a series of Second-order polynomial equations into one of solving many linear equations and a single-variable polynomial equation is discussed in parameter recognition based on current-voltage results[23].

In a range of more than 90 series-connected cells, a Thevenin ECM is used for every single cell to define the internal resistance of each cell[24]. In a Thevenin model, n cells are represented in a series-connected battery pack using two separate charging and discharge branches in series n times and the model equations for n cells are presented as a single device Accordingly, because of their outstanding dynamic efficiency. There have been three distinct ECMs of lithium-ion batteries commonly accepted[25]. which demonstrates that the second-order ECM is the most accurate and has the highest dynamic performance, but still the most complex. Also, in conjunction with an improved EKF[26]and the CC estimation system to estimate the SOC, the classification equations from each of the three models described are introduced and used. For SOC estimation, the Thevenin model and first-order ECM were used and compared to three other improved ECMs[27], and the contrast between these models is the way the SOC equations are measured[28]. Depending on the situation where the model should be used, the parameters of the first-order ECM can be determined for different datasets[29], such as a contrast between continuous-time and discrete-time equations of the second-order ECM[30] is made and concludes that discrete-time recognition approaches are less stable due to undesirable sensitivity issues in the transition of discrete domain par. The transition of the model equations with the implementation of a simple Thevenin ECM can be determined explicitly according to SOC[31]. ECM is used to obtain the OCV as a Thevenin, and then a linear fitting of a component of the OCV-SOC curve is used to obtain the SOC[32]. To obtain the SOC with a basic ECM that considers only a voltage source and an internal resistance, a similar method is used[33].

A Kalman filter (KF) is introduced to extract an OCV value in a noisy environment, and then to estimate SOC based on the OCV–SOC mapping[34], and as it has the observed ability of the system as a requirement, a virtual-measurement-based method can be implemented to account for a local loss of observing ability like in This approach uses the iterative process of the KF for estimating not only SOC but also other battery parameters. For example, both SOC and SOH are estimated in This indicates that there are various types of closed-loop approaches for SOC estimations in addition to models, such as direct feedback improved extended Kalman filters (EKF), unscented Kalman filters (UKF), and neural network[35]. These methods are used to further increase the accuracy of the SOC estimation since the variance of current system state estimates can be calculated recursively and Kalman gain can be adapted to achieve optimum estimation in the next stage[36]. Lithium-ion battery electrochemical and thermal simulations are extremely nonlinear and are thus used by the EKF to approximate battery parameters[37].

It also presents the implementation and use of the EKF algorithm for SOC estimation[38]. To estimate the SOC value, it is normal to use a mixture of CC or OCV methods with the KF method. It is also used in conjunction with CC and/or OCV, as suggested in the EKF process. UKF, which is used in UKF to approximate SOC using a modified ECM with a resistance and capacitor correction factor[39], is another common enhancement to the KF algorithm for finding SOC[40]. This was done to include the effect on the battery internal resistance of various current rates and SOC[41], and the impact on the battery power of different temperatures and current rates. The papers presented the use of a multiple-model method to approximate the SOC of the battery using a bank of IEKF[42].

The Improved Extended Kalman Filter (IEKF) is a pure time-domain filter for nonlinear systems that uses a mathematical recursive formula to provide an effective calculation process[43]. By this process, the state of the target at the next moment can be determined optimally. The Improved Extended Kalman Filter is currently used more and more commonly in the electric vehicle SOC estimate[44]. A new EKF-based SOC

estimation method[45], together with the current optimization method and the open-circuit voltage method, is, therefore, suggested. The high-order equivalent model is used to study the calculation of the vehicle power battery residual energy[46]. This proposes an experimental approach to the identification of parameters of batteries Based on the electric equivalent battery circuit[47], andan Improved Extended Kalman Filter (IEKF) estimator was created. To remove calculation and system noise, this repetitive approach can be used in real-time. For battery systems, this hybrid approach, which is extended here to a continuous system of discrete measurements, is especially appropriate.

2. Mathematical analysis

2.1. High-order electrical equivalent circuit modeling

Equivalent circuit models use a circuit consisting of voltage sources, resistors, and capacitors to simulate the dynamic characteristics of batteries thus describing the relationship between voltage and currently shown in the battery operation. In this paper, a high-order electrical equivalent model is researched, as it refers mostly to the equivalent circuit models used in the literature. On one hand, the high-order electrical equivalent model does a good job of reflecting the dynamic and static characteristics of lithium-ion batteries, and on the other hand, the complexity of the model is also appropriate, easy to implement in engineering, and it is easy to implement parameter identification with high precision.The high-order electrical equivalent circuit, also known as the second-order RC equivalent model, consists of a voltage source and parallel network. There are several types of equivalent circuit models such as the Rint model, the PNGV model, the Thevenin model, the Dual Polarization model, etc. The Thevenin model can accurately describe the battery dynamic behaviors without the complex model structure. In this paper, a High-order electrical equivalent circuit model is considered, as shown in Fig. (1).

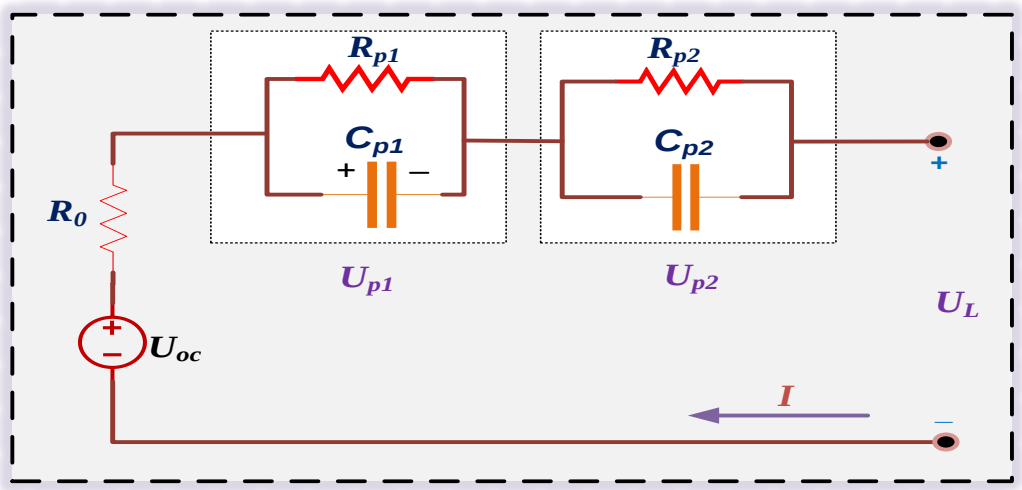

Figure 1. high-order electrical equivalent circuit modeling

The terminal voltage of the battery, $I$is the outflow current, R_0 is the ohmic resistance of the connectors, electrodes, and electrolyte, and the two sets of parallel resistor-capacitor elements connected in series R_{p1}, R_{p2}, and C_{p1}, C_{p2} are the mass transport effects and double-layer effects, respectively. and U_L is the terminal voltage in the circuit. Commonly, the time constants of the two dynamics differ by at least an order of magnitude. According to Kirchhoff's circuit law get the Eq (2).

$$\begin{cases} U_L = U_{oc} - U_{p1} - U_{p2} - (I * R_0) \\ U1 = -\dfrac{U_{p1}}{R_{p1}C_{p1}} + \dfrac{I}{C_{p1}} \\ U2 = -\dfrac{U_{p2}}{R_{p2}C_{p2}} + \dfrac{I}{C_{p2}} \end{cases} \tag{1}$$

As the state variable, (SOC $U_{P1}U_{P2}$) is selected for the specified high-order electrical equivalent model. Its state space equation can be listed as seen in the equation after the discretionary equation (2) and the description of SOC as shown in Eq(3).

$$\begin{cases} \begin{bmatrix} SOC_{k+1} \\ U_{p,k+1} \\ U_{c,k+1} \end{bmatrix} = \begin{bmatrix} 1 & 0 & 0 \\ 0 & e^{(-t/\tau_p)} & 0 \\ 0 & 0 & e^{(-t/\tau_c)} \end{bmatrix} \begin{bmatrix} SOC_k \\ U_{p,k} \\ U_{c,k} \end{bmatrix} + \begin{bmatrix} -t/\eta Q_0 \\ R_p\left(1\text{-}e^{(-t/\tau_p)}\right) \\ R_c\left(1\text{-}e^{(-t/\tau_c)}\right) \end{bmatrix} I(k) \\ U_{k+1} = U_{oc}(SOC_{k+1}) - U_{p,k+1} - U_{c,k+1} - iR_o \end{cases} \quad (2)$$

In the above equation, R_{p1}, C_{p1}, and R_{p2}, C_{p2} are cut-off angular frequencies. Hybrid Pulse Power Characteristic (HPPC) is selected to conduct the test experiment of Hybrid Pulse Power Characteristic (HPPC). According to the changes in the external characteristics of lithium batteries, it uses MATLAB to carry out offline parameter identification using the least-squares principle. It can also curve fit the data according to the cftool in MATLAB to get the identified parameters.

2.2. Parameter Identification of the high-order circuit model

Parameter detection of the battery equivalent circuit model includes the determination of the battery OCV, the ohmic resistance, and the parallel resistor-capacitor parameters at various SOC. The tests performed are usually constant current pulse discharge or charge tests. Since the model parameters are functions of battery SOC, for parameter identification at each SOC, the discharge or charge pulse is set short so that the SOC and all the model parameters can be considered constant during the testing.

The test data for SOC at 0.9 can be obtained by using the experimental results from the OCV and HPPC tests as the basis for parameterization. The values for various segments of the curve corresponding to the battery during the experiment are represented by the labels U1 to U8. U1–U4 and U5–U8 represent the battery's discharge and charging characteristics, respectively as shown in Fig. (2).

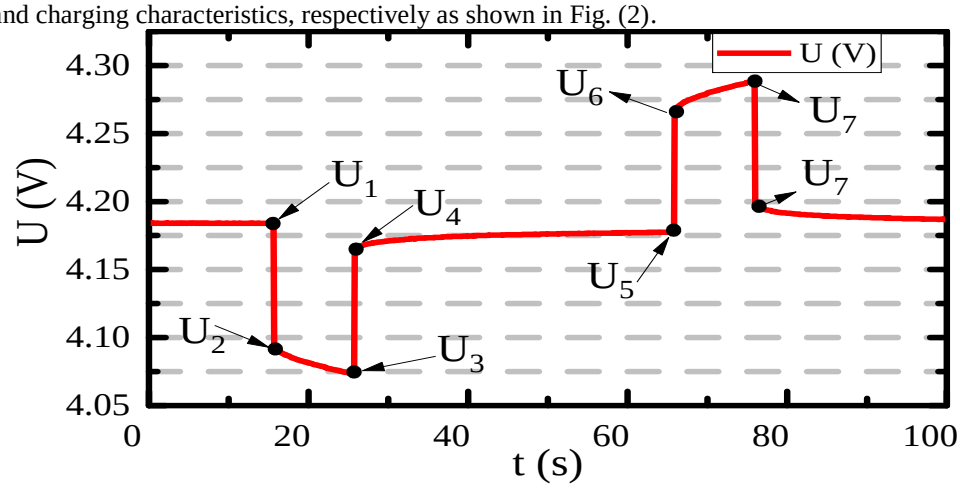

Figure 2: voltage curve for a specific SOC

The ohmic internal resistance can be considered as a unique factor that causes the voltage drop at the moment. The ohmic resistance can be shown in Eq (3).

$$R_0 = \frac{U1 - U2}{I} \quad (3)$$

The ohmic internal resistance can be considered as a unique factor that causes the voltage drop at the moment. An efficient method of processing is used to create a relationship between the internal parameters of the equivalent circuit model and the state of charge. Also, the values of the remaining parameters can be obtained by integrating. However, compared with the co-efficient, the values of the parameters can be obtained in Eq (4).

$$\begin{cases} R_p = \dfrac{U_1 - U_2}{I}, C_p = \dfrac{\tau}{R_p} \\ R_{p1} = \dfrac{U_2 - U_3}{i}, C_{p1} = \dfrac{dU_{p1}}{dt} + \dfrac{U_{p1}}{R_{p1}} \times i \\ R_{p2} = \dfrac{U_4 - U_5}{i}, C_{p2} = \dfrac{dU_{p2}}{dt} + \dfrac{U_{p2}}{R_{p2}} \times i \end{cases} \tag{4}$$

In the high-order electrical equivalent circuit model, these equations are the values of any parameter. During the data analysis and processing process, the thriving data section is derived from the initial experimental data, and then the extracted data segment is analyzed. The parameters of τ_1 and τ_2 where the two-time constant is calculated, as shown in Eq(5).

$$\begin{cases} \tau_1 = R_{p1} \times C_{p1} \\ \tau_2 = R_{p2} \times C_{p2} \end{cases} \tag{5}$$

2.3. Improved Extended Kalman filter

The improved extended Kalman filter algorithm is a nonlinear linear process. By estimating the value of the next moment from the previous time, the observation value of the input and output of the system is applied to continuously update, to achieve the optimal estimation. When using the improved extended Kalman filter method to estimate the SOC of a lithium battery, the process noise, and the observed noise are required to be white noise of a Gaussian distribution. In this case, the process noise and the process noise can be facilitated. The covariance of the observed noise is controlled. In the estimation process, the Taylor expansion algorithm is applied to unfold the system model of the lithium battery, and then the first-order linearization model is left after the high-order term is removed. After obtaining the linearization model, the SOC of the lithium battery is further estimated by the Kalman filter, and the algorithm flow of the improved extended Kalman is shown in Fig. (3).

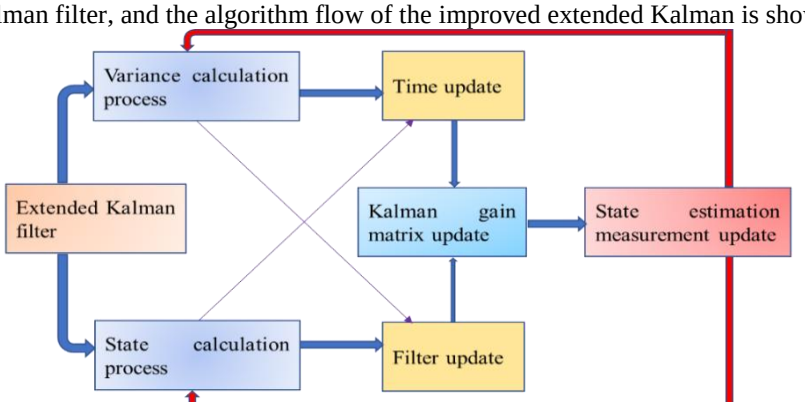

Figure 3. IEKF-based calculation process

At the time of *k*, it is assumed that the covariance of the *k-1* state estimation values and the estimation errors at the previous time has been obtained. The time *k* is now predicted in advance by the state values of *k-1* moments. In the mathematical model, the latter moment is a function of the previous moment. Therefore, combining the system state at the previous moment with the error covariance and the Kalman gain, a priori prediction value for the current time can be obtained. The two values written before and after the model are true values, and the true value is not available under actual conditions. The posterior state estimate is used at the previous moment, so it is also necessary to predict the next step in advance. The value. According to the measurement function in the mathematical model, the measured true value is a function of estimating the true value, but in actual cases, the estimated true value cannot be obtained, and there is no noise. In the case of linearization error, the value calculated by the mathematical model and the physical value directly measured by the physical method, the measured true value is equal, because the linearization error of the mathematical model

plus the prior estimate There is a certain error between the value and the estimated value. There is a certain error between all the measured values obtained by the mathematical model and the actual measured true values. In this case, system noise and process noise are generally approximated as white noise following a Gaussian distribution. A Kalman filter that linearizes the expectation and covariance of system noise and process noise during the estimation process.

The improved extended Kalman algorithm is an improvement to the classical Kalman algorithm. It is to spread the nonlinear space equation through Taylor, round off the second-order and above high-order terms, obtain the approximate linear space equation, and then apply the Kalman filter algorithm to the linear space equation to estimate the current spatial state, suitable for a discrete non-distribution linear system. The expression equations and observation equations of the discrete nonlinear system space as shown in Eq (6).

$$\begin{cases} X_{k+1} = f(X_k, k) + w_k \\ Z_k = h(X_k, k) + v_k \end{cases} \tag{6}$$

The first part of the equation represents the state equation, and the second part represents the observation equation. K is discrete-time, X_{k+1} is an n-dimensional state vector, $Z_k$is an m-dimensional observation vector, and w_k and $v_k$are mutually independent Gaussian white noise. To apply the Kalman filter, the first-order Taylor expansion is performed on the nonlinear functions f (*) and h (*) around (Xk), and the expansion result is shown in Eq(7).

$$\begin{cases} f(X_k, k \approx f(\hat{X}_k, k) + \left.\dfrac{\partial f(X_k, k)}{\partial X_k}\right|_{X_k = \hat{X}_k} (X_k - \hat{X}_k) \\ h(X_k, k) \approx h(\hat{X}_k, k) + \left.\dfrac{\partial h(X_k, k)}{\partial X_k}\right|_{X_k = \hat{X}_k} (X_k - \hat{X}_k) \end{cases} \tag{7}$$

For the formula (6), the values of AK, BK, CK, and DK as shown in Eq (8)

$$\begin{cases} A_k = \left.\dfrac{\partial f(X_k, k)}{\partial X_k}\right|_{X_k = \hat{X}_k} \\ B_k = f(\hat{X}_k, k) - A_k \hat{X}_k \\ C_k = \left.\dfrac{\partial h(X_k, k)}{\partial X_k}\right|_{X_k = \hat{X}_k} \\ D_k = h(\hat{X}_k, k) - C_k \hat{X}_k \end{cases} \tag{8}$$

The recursive process of the improved extended Kalman filter is obtained by applying the Kalman filter basic equation as shown in Eq(9).

$$\begin{cases} \hat{X}^-_{k+1} = f(\hat{X}_k) \\ \hat{P}^-_{k+1} = A_k \hat{P}_k A_k^T + Q_{k+1} \\ K_{k+1} = \hat{P}^-_{k+1} C^T_{k+1} (C_{k+1} \hat{P}^-_{k+1} C^T_{k+1} + R_{k+1})^{-1} \\ \hat{X}_{k+1} = X^-_{k+1} + K_{k+1} \left[Z_{k+1} - h(X^-_{k+1}) \right] \\ \hat{P}_{k+1} = [I - K_{K+1} C_{k+1}] P^-_{k+1} \end{cases} \tag{9}$$

Where P is the mean square error and K is the Kalman gain. $I$is an $n \times m$ unit array. Q and R are the variances of w and v, respectively, and generally do not change with the system. The initial value of the filter and the filter variance are X (0) = E [X (0)], and P (0) = var [X (0)], respectively. The filtering step in the $(k+1)$

period is as follows: firstly, the state of the current time and the mean square error are estimated from the state $X\hat{}_k$ at k time and the mean square error *(P k)* to obtain a prior state ($X\_(k+1)$^- *)* ˆand the prior mean squared error $P\_(k+1)$^-, then calculate the Kalman gain K_{k+1} at the current moment. Finally, the state of the current time ($X\_(k+1)$ is obtained by correcting the prior state with K_{k+1}, and the mean squared error of the current time is obtained by correcting the a priori mean square error ($P\_(k+1)$)ˆ.

2.4. IEKF iterative calculation process

While the EKF increases the algorithm's ability to deal with nonlinear processes, it also needs to be improved further for complex machine state monitoring problems in real-world applications. The system noise in real-world battery packs, such as the constant divergence of the current and voltage sensors, is often non-Gaussian, particularly for large volume battery packs. Furthermore, battery capacity loss, atmospheric temperature, and complex operating conditions are all closely linked to the characteristics, impacting the precision and robustness of the SOC calculation. As a result, any optimization is used to boost the EKF algorithm to reduce the effects of the above variables.

Adaptive noise: Signal noise can be divided into process noise and ambient noise with the Kalman filter. The ambient noise is also caused by errors caused by the sensor and environmental interference during the actual calculation, and the process noise characterizes the model's efficiency. Both noises have a significant effect on the filtering system's efficiency, primarily affecting the system's convergence and accuracy. The scheme is known to be converted to a constant value at an infinite moment for a converged Kalman filter as shown in Eq(10).

$$\lim_{k \to \infty} P_k = P_{const} \tag{10}$$

The Kalman Gain, like the convergent covariance matrix, converges to a constant value according to the covariance matrix updating the EKF. As a result, the Kalman filter degrades to a low-pass filter, with the Kalman Gain calculated solely by machine noise, which affects precision.

*Process noise:*on the other hand, affects the system's convergence level. Where there is a divergence, the presence of noise will help the device eventually converge to the true value, with the speed of convergence depending on the amplitude of the noise.For discrete systems, the adaptive algorithm based on maximum posterior estimation can be defined as Eq(11) and (12).

$$\begin{cases} \hat{w}_k = (1-d_k)\hat{w}_{k-1} + d_k(\hat{x}_k - (A\hat{x}_{k-1} + Bu_k)) \\ \hat{v}_k = (1-d_k)\hat{v}_{k-1} + d_k(z_k - C_k x_k) \end{cases} \tag{11}$$

$$\begin{cases} \hat{Q}_k = (1-d_k)\hat{Q}_{k-1} \\ +d_k(G_k \varepsilon\varepsilon^T G_k^T + P_k - A_{k-1}P_{k|k-1}A_{k-1}^T) \\ \hat{R}_k = (1-d_k)\hat{w}_{k-1} \\ +d_k(\varepsilon\varepsilon^T - C_k P_{k|k-1} C_k^T) \end{cases} \tag{12}$$

where $d_k = (1-b)/(1-b_k)$, b is a constant between 0 and 1, $\varepsilon = z_k - C_k x_k$.

Fading filter:For the arbitrary time k in the time domain, traditional EKF algorithms conclude that the complete filtering time domain is N, thus we have:

$$P_{k|k-1}^N = A_{k-1} \Big| P_{k-1}^N A_{k-1}^T + Q_{k-1} \tag{13}$$

Take s as the fading factor, and multiply both sides of the Eq. (14) by $s^{-(N-k)}$:

$$s^{-(N-k)} P_{k|k-1}^N = A_{k-1}(s^{-(N-k)} P_{k-1}^N) A_{k-1}^T + Q_{k-1} \tag{14}$$

Note:

$$P_{k|k-1}^{N*} = s^{-(N-k)} P_{k|k-1}^N \tag{15}$$

$$P_{k-1}^{N*} = s^{-(N-(k-1))} P_{k-1}^{N} \tag{16}$$

Then Eq. (14) can be expressed as Eq. (17)

$$P_{k|k-1}^{N*} = A_{k-1}(sP_{k-1}^{N*})A_{k-1}^{T} + Q_{k-1} \tag{17}$$

To optimize the covariance matrix updating, Eq. (17) may be substituted for Equation (13), and the covariance matrix has been expanded by s times as opposed to the initial equation, indicating that the calculation capacity has been improved.

Eq. (17)'s a fading factor can be set to a value greater than 1, and it can also be adaptively modified based on the degree of device model mismatch. Furthermore, the error bars are visible.

Linear-nonlinear filter:As the EKF is increased by combining multiple solutions, the algorithm's computation cost rises, making quick estimation impossible. As a result, the linear–nonlinear (L–N) filter is used to solve problems caused by the algorithm's complexity.

Noting that the second-order ECM has the following characteristics:

1. The state update process is linear.

$$x(k+1) = Ax(k) + w(k) \tag{18}$$

2. Observation process is non-linear.

$$x(k+1) = Ax(k) + w(k) \tag{19}$$

The observation method concentrates on the nonlinear proportion. As a result, the state update section is assumed to be processed independently from the observation portion. When working with linear systems that need little estimation, traditional Kalman filtering has higher precision. However, while the EKF can respond to nonlinear systems when dealing with linear systems, the accuracy is close to that of classical Kalman filtering, and a lot of computational power is wasted. As a result, the L-N filter is used to solve the problem for the special linear-nonlinear method described earlier. For the status updating process, the classical Kalman filter method is used, and the EKF is used for the observation process, which essentially decreases the amount of computation needed by the algorithm without impacting estimation accuracy.

Table 1: Improved EKF algorithm

Initialization:	
	$\hat{X}_0 = E[X_0]$
	$P_0 = E[(X - \hat{X}_0)(X - \hat{X}_0)^T]$ $\hat{V}_0 = E(V_0)$ $\hat{W}_0 = E(W_0)$ $s = s_0$
Prediction:	
Status prediction	$x_{k\|k-1} = Ax_{k-1} + Bu_k + w_{k-1}$
Covariance matrix prediction	$P_{k\|k-1} = A_{k-1}(s.P_k)A_{k-1}^T + Q_{k-1}$
Updating:	
Observation	$\hat{z}_k = g(x_k, u_k, v_k)$
Kalman gain matrix (K)	$K_k = P_{k\|k-1}C_k^T(C_k P_{k\|k-1} C_k^T + R_{k-1})^{-1}$
Where:	$C = \left.\begin{bmatrix} \frac{\partial g_1}{\partial x_1} & \frac{\partial g_1}{\partial x_n} \\ \frac{\partial g_m}{\partial x_1} & \frac{\partial g_m}{\partial x_n} \end{bmatrix}\right\|_{x=\hat{x}_{k\|k-1}}$

Status update	$\hat{x}_k = \hat{x}_{k\|k-1} + G_k(z_k - \hat{z}_k)$
Covariance matrix update	$P_k = (I - G_k C_k) P_{k\|k-1}$
Noise adaptation	$\begin{cases} \hat{w}_k = (1-d_k)\hat{w}_{k-1} \\ +d_k(\hat{x}_k - (A\hat{x}_{k-1} + Bu_k)) \\ \hat{v}_k = (1-d_k)\hat{v}_{k-1} \\ +d_k(z_k - \hat{z}_k) \end{cases}$
	$\begin{cases} \hat{Q}_k = (1-d_k)\hat{Q}_{k-1} \\ +d_k(G_k \varepsilon\varepsilon^T G_k^T + P_k - A_{k-1}P_{k\|k-1}A_{k-1}^T) \\ \hat{R}_k = (1-d_k)\hat{w}_{k-1} \\ +d_k(\varepsilon\varepsilon^T - C_k P_{k\|k-1} C_k^T) \end{cases}$

Several methods for dealing with filtering noise and divergence problems are introduced in the improved extended Kalman filter. To minimize the sum of estimation, the L–N filter approach is used. The improved extended Kalman filter algorithm adopted can be described as Tab. (1).

3. Experimental analysis

3.1. Test platform construction

In this experiment, a lithium cobalt oxide battery with a rated capacity of 70 Ah was selected as the experimental object. The basic technical parameters are shown in Table 1. Battery HPPC experimental charging and discharging equipment is the power battery large-rate charge and discharge tester (CT-4016-5V100A-NTFA). The incubator is a three-layer independent temperature control high and low-temperature test chamber (DGBELL BTT-331C), and the experiment was carried out at a constant temperature of 25 °C. HPPC test platform is sowing in Fig. (4).

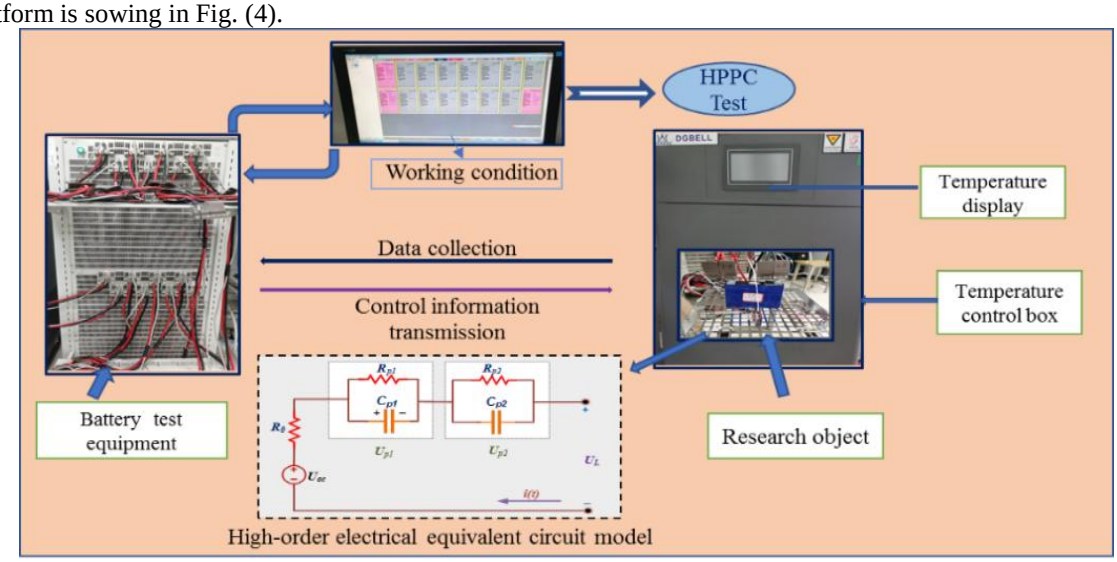

Figure 4. platform design for HPPC test

In this experiment, the lithium ternary battery is selected as the experimental project. The basic technical parameters of the battery are shown in Tab. (2)

Table 2. Basic technical parameters of the battery

Factor	parameter
Size: length * width * height /mm	200*80*180
Rated voltage/V	3.7
Maximum load current /A	1.5C
Charge cut-off voltage/V	4.2
Discharge cutoff voltage/V	2.75
Working temperature /°C	25°C
Rated capacity/Ah	70

3.2. HPPC test steps

The HPPC (Hybrid Pulse Power Characterization) test is intended to determine dynamic power capability over the device's useable voltage range using a test profile that incorporates both discharge and regen pulses. In this analysis, the battery at ambient temperature was subjected to HPPC and the parameters of the battery model were obtained by examining the battery's operating characteristics during operation. The following are the basic experimental steps of the HPPC experiment in Fig. (5).

ID	Step name	Step Time	Voltage (V)	Current (I)	Capacity (Ah)
1	CCCV_ Chg		4.2	70	
2	Rest	00:40:00:000			
3	CC_DChg	00:00:10:000		70	
	Record	Time section	0 sec	10sec	Time 0.1sec
4	Rest	00:00:40:000			
	Record	Time section	0 sec	40sec	Time 0.1sec
5	CC_DChg	00:00:10:000		70	
	Record	Time section	0 sec		
6	Rest	00:05:00:000			
7	CC_DChg	00:06:00:000		70	
8	Cycle	Begin ID: 2	Times 9		
9	End				

Figure 5.step-settings for HPPC test

The battery was completely charged first and then left for 30 mins to rest. A discharge pulse of 10 seconds is executed and left to rest for 40 minutes, then a charge pulse of 10 seconds is executed and left to rest for 30 minutes. This is replicated nine (9) times, and to define the parameters in the circuit, data is registered at various SOC stages. The measurement was performed from 0.9 to 0.1 at 0.1 SOC intervals. When a current is loaded, there is a pulse charge or discharge, a voltage increases or decrease occurs and this can be used to measure the parameters.

3.3. Hybrid pulse-Power characteristic test and validation

The hybrid pulse-power test method exhibits a change in battery voltage as a function of the battery charge-discharge conditions, which reflects the dynamic battery characteristics of operation. The key parameters required for the equivalent circuit model can be easily determined by the hybrid pulse-power test. The hybrid pulse-power test detects the internal ohmic resistance of the battery by dynamically changing its terminal voltage at the beginning and end of the charge-discharge treatment. After that, the internal voltage is slowly changed to detect and determine the internal polarization resistance and capacity values.The hybrid pulses test

consists of a sequence of Hybrid Pulse Power Characterization (HPPC) profiles with constant-current discharged pulses and rests. A lithium-Ion cell with a capacity of 70 Ah and a nominal voltage of 3.65 V is tested in this paper. The data acquisitions of the HPPC test include SOC-OCV, load current, and terminal voltage as shown in Figures (6). The load current is used as the input to validate the battery model. The simulated terminal voltage is compared with the measured voltage in Figure 14. The hybrid pulse-power test experimental renderings are shown in Fig. (6).

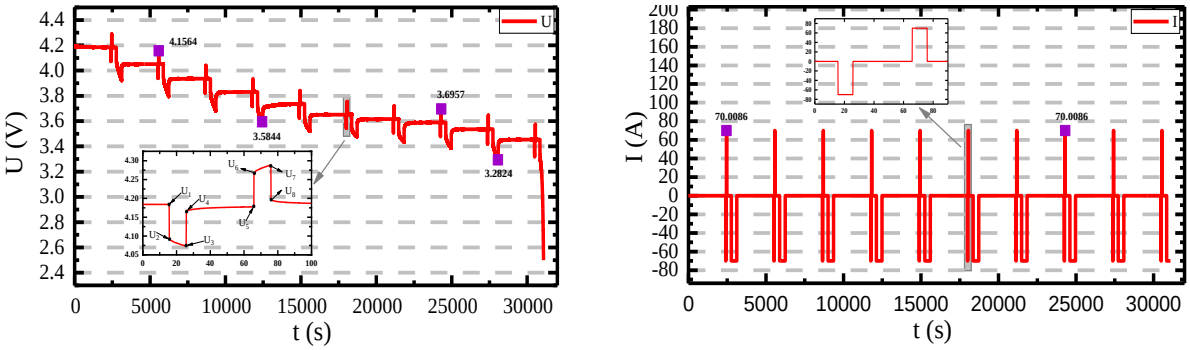

(a). EKF estimation results with SOC (b). EKF estimation error with SOC

Figure 6.load current pattern and terminal voltage response of the HPPC test

3.4. Experimental results explanation

The experimental results are shown in Table 2. According to the HPPC experimental data of each SOC test point, the values of the parameters in the high-order circuit model corresponding to the SOC value can be obtained as shown in the table. (3).

Table 3.Parameter detection from HPPC test

SOC	*OCV*	R_0	R_p	R_{P1}	R_{p2}	C_p	C_{p1}	C_{p2}
0.1	4.1840	0.001311429	0.000384286	0.000559143	4.47857E-05	23758.36	33873.27542	33873.27542
0.2	4.0513	0.001302857	0.000414286	4.24286E-05	0.000539286	21033.79	21575.08418	21575.08418
0.3	3.9360	0.001302857	0.000456571	0.000715857	5.37714E-05	20340.74	29419.27759	29419.27759
0.4	3.8309	0.001302857	0.000481857	0.0000429	0.000638429	19989.33	18857.80886	18857.80886
0.5	3.7366	0.001305714	0.000482857	0.000590857	3.97714E-05	19245.86	23914.41006	23914.41006
0.6	3.6511	0.001311429	0.000300714	0.000338143	2.64286E-05	26486.94	31850.4436	31850.4436
0.7	3.6163	0.001324286	0.000309857	7.43857E-05	0.001505714	27796.68	26980.98713	26980.98713
0.8	3.5900	0.001351429	0.000326286	0.000378429	2.88714E-05	26145.8	31657.22914	31657.22914
0.9	3.5367	0.001395714	0.000387143	0.000468143	3.76714E-05	22668.63	28153.79921	28153.79921
1	3.4545	0.001478571	0.000556714	0.000101071	0.000695429	12521.68	4507.70318	4507.70318

Parameter detection by curve fitting in MATLAB was used to get the polynomial relationship between SOC and OCV. The relationship between the SOC and the battery parameter can be obtained by fitting a sixth-order polynomial regression model (as shown below) to the experimental data using the least-squares method. Parameter detection by curve fitting in MATLAB was used to get the polynomial relationship between SOC and OCV, R_0, R_{p1}, R_{p2}, C_{p1}, C_{p2} are shown in Eq (20).

$$\begin{cases} \begin{cases} f(OCV) = 34.13*u^6 - 109.8*u^5 + 133.8*u^4 - 75.6*u^3 + 19.72 \\ *u^2 - 1.512*u + 3.4545 \end{cases} \\ \begin{cases} f(R0) = -0.01927*u^6 + 0.05584*u^5 - 0.05832*u^4 + 0.02462 \\ *u^3 - 0.001883*u^2 - 0.001503*u + 0.001678 \end{cases} \\ \begin{cases} f(Rp1) = 0.1934*u^6 - 0.6239*u^5 + 0.7864*u^4 - 0.4981*u^3 + \\ 0.1707*u^2 - 0.03068*u + 0.002743 \end{cases} \\ \begin{cases} f(Rp2) = 0.03677*u^6 - 0.132*u^5 + 0.1886*u^4 - 0.1375*u^3 + \\ 0.05426*u^2 - 0.01103*u + 0.0009403 \end{cases} \\ \begin{cases} f(Cp1) = 3.568e+06*u^6 - 1.338e+07*u^5 + 1.911e+07*u^4 \\ -1.281e+07*u^3 + 3.938e+06*u^2 - 4.261e+05*u + 2.593e+04 \end{cases} \\ \begin{cases} f(Cp2) = 4.378e+06*u^6 - 1.406e+07*u^5 + 1.766e+07*u^4 \\ -1.089e+07*u^3 + 3.349e+06*u^2 - 4.347e+05*u + 2.084e+04 \end{cases} \end{cases} \tag{20}$$

The proposed high-order electrical equivalent circuit's internal Ohmic resistance R_0, electrochemical polarization resistance R_{p1}, and concentration polarization resistance R_{p2} are compared. The relationship between the SOC and the battery parameter can be obtained by fitting a sixth-order polynomial regression model as shown in Fig.(7).

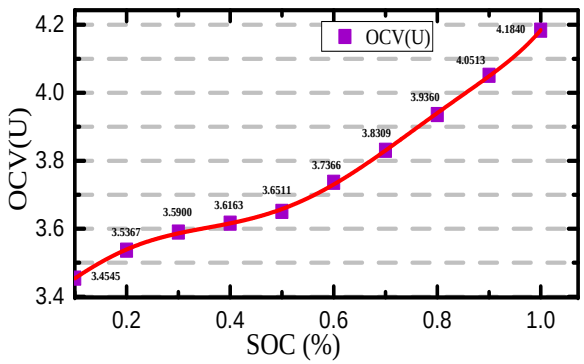

(a) Relation between SOC and OCV

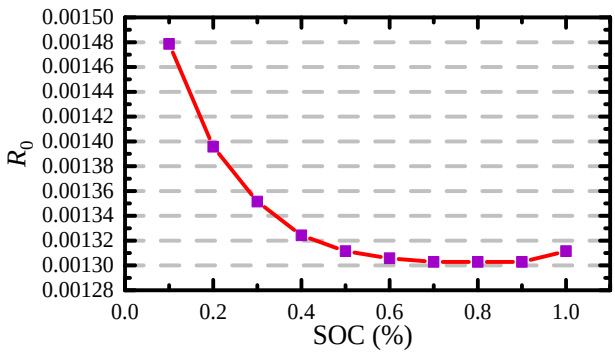

(b) Relation between SOC and R_0

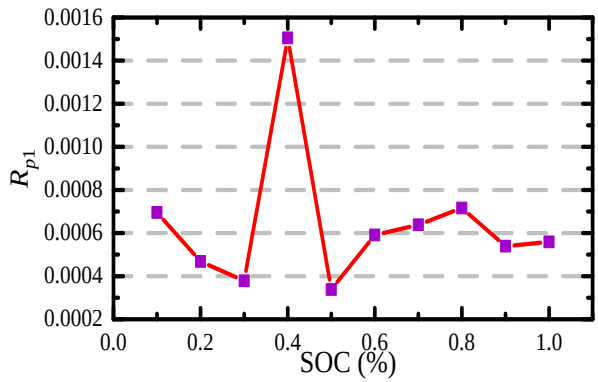

(c):Relation between SOC and R_{p1}

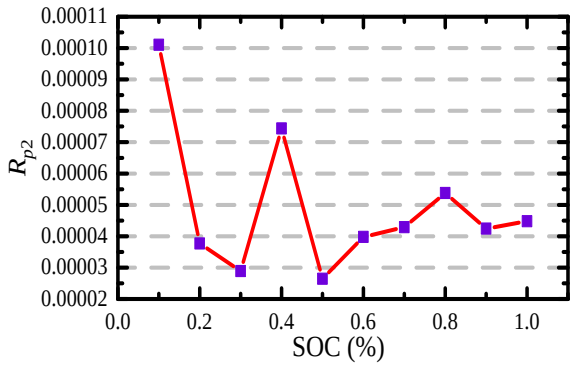

(d): Relation between SOC and R_{p2}

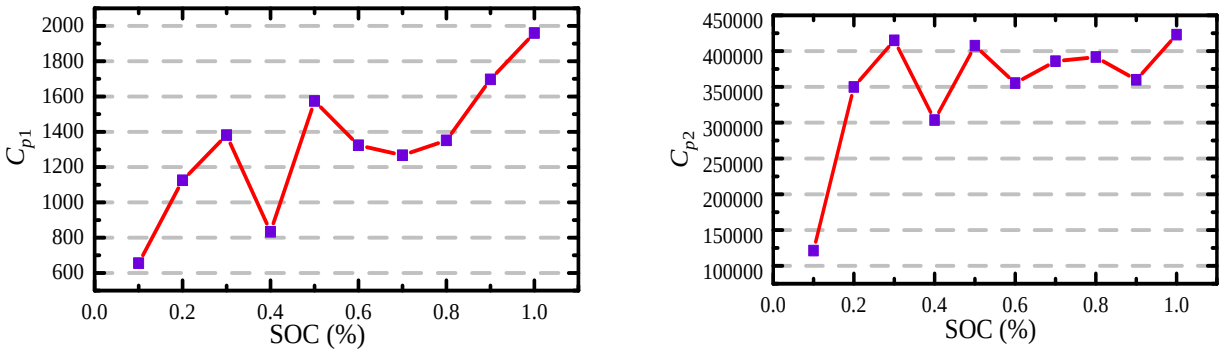

(e): Relation between SOC and C_{p1} (f): Relation between SOC and C_{p2}

Figure 7: Relationship between SOC, OCV, and others parameter

According to the internal resistance, R_0 decreases steadily as the state-of-charge increases. The electrochemical polarization resistance R_{p1}first increases and then decreases with a decreasing SOC and then increases again as SOC approaches the lowest point. The concentration polarization resistance R_{p2}first decreases then increases sharply and gently decreases as SOC decrease as shown in Fig. 7 (b, c). The values of the electrochemical polarization capacitance C_{p1} and the concentration polarization capacitanceC_{p2} calculated from the proposed high-order electrical equivalent circuit are compared in Fig. 7 (d, c).

3.5. Experimental verification

The simulation system model is established to verify the state estimation effect of the algorithm. The current and voltage data obtained from the experimental test are imported into the model. The parameterization of the high-order electrical equivalent circuit model is based on the HPPC experimental findings. The findings are compared with and the results from the HPPC experiment and the computations performed afterward to validate the validity of the SOC predicted values in the simulation. The simulation terminal voltage is calculated using the simulation model, and the experimental terminal voltages are compared to arrive at the final result. The value of current (I) in the experimental data obtained by the test instruments is used as the input state, and the simulation terminal voltage is obtained through to the simulation model and the experimental terminal voltages are compared to obtain. The simulation verification model is shown in Fig. (8).

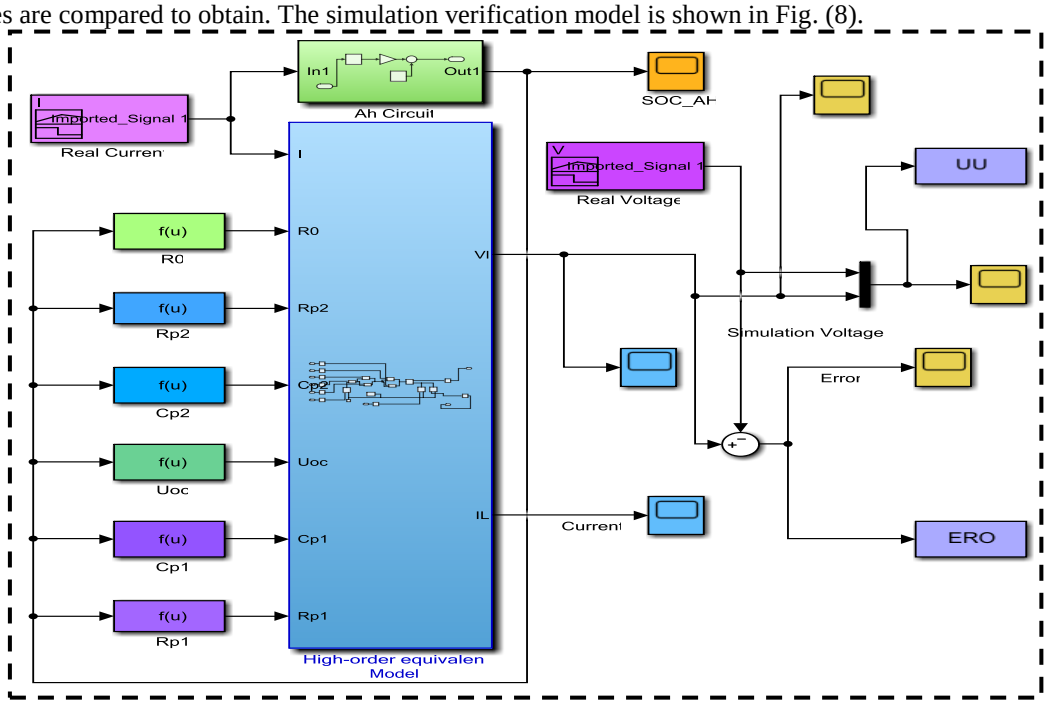

Figure 8. simulation verification model with block

The simulation system model is established to verify the state estimation effect of the algorithm. The current and voltage data obtained from the experimental test are imported into the model. The simulation part is mainly to write the s-function module of the improved program. According to this model, the simulation verification result and Error of this Experiment are given below.

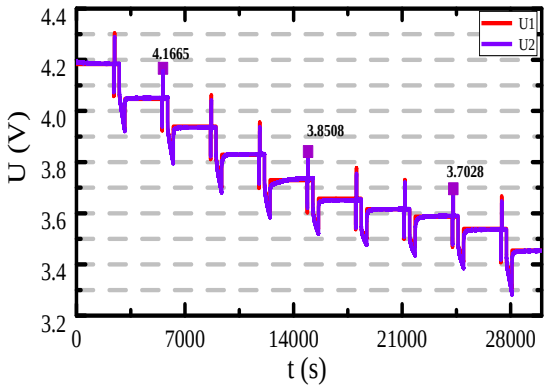

a. simulation verification results by traditional model

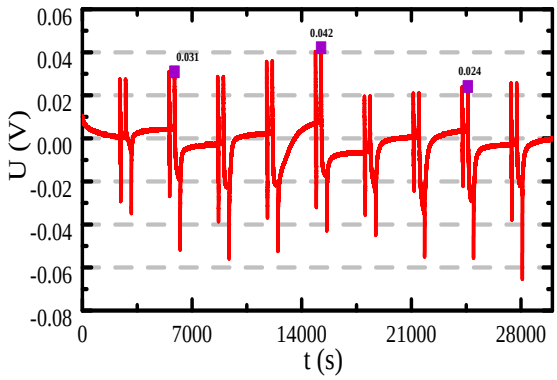

b. simulation verification error by the traditional model

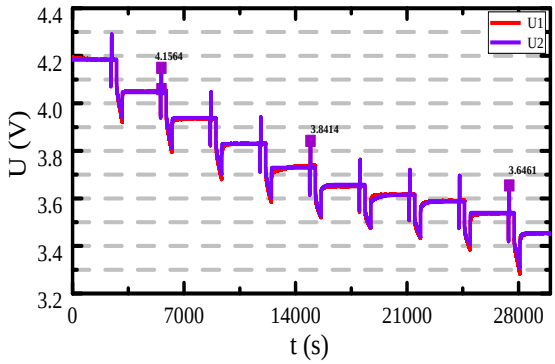

c. simulation verification results by the proposed model

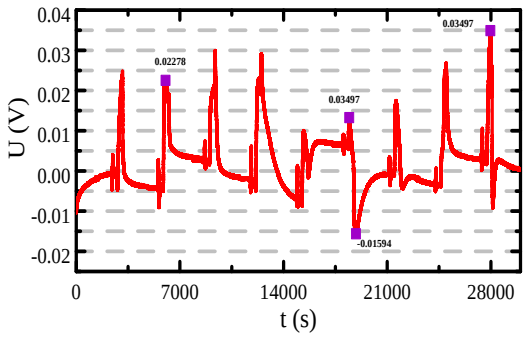

d. simulation verification error by the proposed model

Figure 9: simulation verification result and error comparison

In figure 9 (a) U_1 is the change curve of real terminal voltage data obtained by the traditional equivalent circuit model during the HPPC test. U_2 is the output terminal voltage curve obtained from the simulation model. Figure 9 (b) is the error curve obtained through the difference in voltage value curves which one is gained by the traditional equivalent model. Here the maximum error is 0.042V.

In figure 9 (c) U_1 is the change curve of real terminal voltage data obtained through the HPPC test by the high-order electrical equivalent circuit model. Form while U_2 is the output terminal voltage curve obtained through the simulation model. Figure 9 (d) is the error curve obtained through the difference in voltage value curves which one is gained by the high-order electrical equivalent model. Here the maximum error is 0.034V. this error is less than the traditional equivalent circuit model error. the simulation system model is established to verify the state estimation effect of the algorithm. The current and voltage data obtained from the experimental test are imported into the model. The simulation part is mainly to write the s-function module of the improved program. According to this model, the simulation verification result and Error of this Experiment are given below.

3.6. IEKF response SOC verification

Using the improved extended Kalman filter method to estimate the SOC of a lithium battery, the process noise, and the observed noise are required to be white noise of a Gaussian distribution, which is a limitation of all Kalman filtering methods.

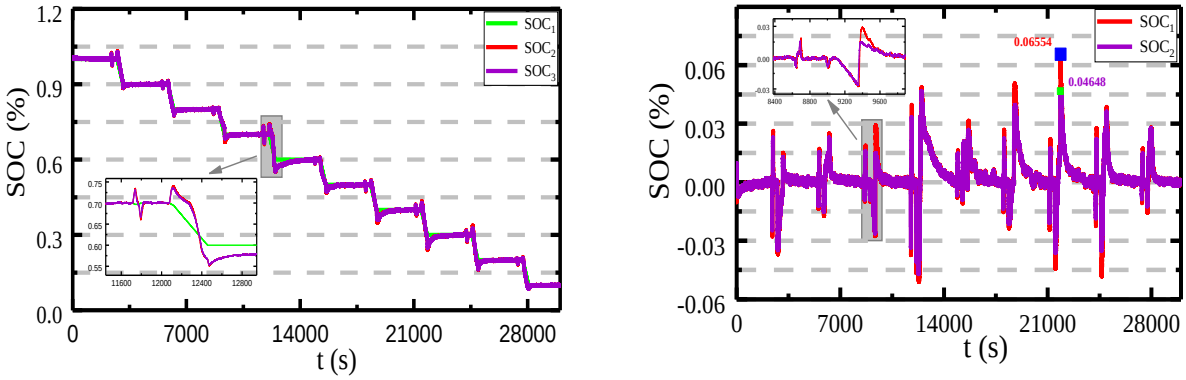

(a). EKF estimation results with SOC (b). EKF estimation error with SOC

Figure 10: IEKF verification result and error comparison

Figure 10 (a) is the result of SOC estimation for three different methods. SOC_1 is the true SOC value, and SOC_2 is the SOC estimate using the traditional equivalent model with an improved extended Kalman algorithm and SOC_3 is the SOC estimation using the high-order electrical equivalent model with an improved extended Kalman algorithm.

Figure 10 (b) is the error curve obtained through the difference in SOC value curves. The error of SOC estimation using the traditional equivalent model with improved extended Kalman algorithm (SOC_1) is less than 2.96%, and the error of SOC estimation using the high-order electrical equivalent model with improved extended Kalman algorithm (SOC_2) is less than 1.83%. which has a good effect on the battery state estimation.

The simulation results show that the high-order electrical equivalent circuit model accuracy under HPPC conditions can reach more than 98.17%. Based on the improved EKF algorithm, where traditional equivalent circuit model accuracy is around 97.4%. According to the simulation results, the main factor of SOC estimates is to accurately identify the parameters. This study showed that in the case of SOC estimation by using an improved EKF algorithm, the high-order electrical equivalent circuit model is more able to accurately identify the parameters than the traditional equivalent circuit model. Due to which the level of error is less in the case of accurate SOC estimation. This means that the use of a high-order electrical equivalent circuit model with improved EKF is able for more error-free than the use of EKF with a traditional equivalent circuit model for accurate SOC estimation.

4. Conclusions

The high-order electrical equivalent model was developed and the parameters were obtained to increase the precision and reliability of estimating the state of charge of lithium-ion batteries This model was selected for power battery charging and discharging because of its low error, long-term testing, polarization effect accounting, and transient analysis. The steps of the experiment were simple and fast, and the algorithm complexity was minimal, resulting in detailed and adequate experimental results for parameterization. The use of an adaptive rule for the process noise covariance matrix improves the accuracy of estimation. The results show that the maximum relative errors of used high-order electrical equivalent circuit model with Improved extended Kalman filter algorithm were 1.83%, which meets the precision criteria for realistic engineering calculations. The error of SOC estimation using the traditional equivalent model with an improved extended Kalman filter algorithm was 2.96%. Which is more flawed than the level of error in the SOC estimate of the proposed method. The high-order electrical equivalent circuit model effectively understands the state of charge calculation of the battery while reducing the effect of nonlinear equations. The findings show that this approach has a greater estimation effect than the traditional equivalent circuit model. The findings have significant implications for the implementation of high-order electrical equivalent circuit simulation of batteries in functional control systems. The improved extended Kalman filtering algorithm is suitable and convenient for SOC estimation because it has reasonable convergence speed, higher estimation precision, and stability. As a

result, for challenging applications such as automobile and high-power systems, the high-order model could be the best option. The use of a high-order electrical equivalent circuit model with an Improved EKF algorithm for SOC estimation will provide more reliable and timely data.

Acknowledgments

The work is supported by the National Natural Science Foundation of China (No. 61801407), Sichuan science and technology program (No. 2019YFG0427), China Scholarship Council (No. 201908515099), and Fund of Robot Technology Used for Special Environment Key Laboratory of Sichuan Province (No. 18kftk03)

References

[1] Yu, Y.X., Y. Song, and J.S. Mao, Quantitative analysis of the material, energy and value flows of a lead-acid battery system and its external performance. *Science of the Total Environment, 2019.* ***688****: p. 103-111.*

[2] Das, U.K., et al., Advancement of lithium-ion battery cells voltage equalization techniques: A review.*Renewable & Sustainable Energy Reviews, 2020.* ***134****.*

[3] Venugopal, P. and T. Vigneswaran, State-of-Health Estimation of Li-ion Batteries in Electric Vehicle Using IndRNN under Variable Load Condition.*Energies, 2019.* ***12****(22).*

[4] Eisa, S. and A. Moreira, A Behaviour Monitoring System (BMS) for Ambient Assisted Living.*Sensors, 2017.* ***17****(9).*

[5] Yan, M., et al., A comprehensive life cycle assessment on dual-source pure electric bus.*Journal of Cleaner Production, 2020. 276.*

[6] Rajagopal, R. and K.S. Ryu, Evaluation of Li6P2S8I solid electrolyte for all solid-state lithium battery applications.*Chemical Engineering Journal, 2020. 402.*

[7] Kwak, M., et al., Parameter Identification and SOC Estimation of a Battery Under the Hysteresis Effect.*Ieee Transactions on Industrial Electronics, 2020.* ***67****(11): p. 9758-9767.*

[8] Shen, J.W., et al., State of charge estimation framework for lithium-ion batteries based on square root cubature Kalman filter under wide operation temperature range.*International Journal of Energy Research, 2020.*

[9] Heo, S., J.H. Jung, and C.G. Park, Consistent EKF-Based Visual-Inertial Navigation Using Points and Lines.*Ieee Sensors Journal, 2018. 18(18): p. 7638-7649.*

[10] Jung, S. and H. Jeong, Extended Kalman Filter-Based State of Charge and State of Power Estimation Algorithm for Unmanned Aerial Vehicle Li-Po Battery Packs.*Energies, 2017. 10(8).*

[11] Wang, D.F., et al., A lithium-ion battery electrochemical-thermal model for a wide temperature range applications.*Electrochimica Acta, 2020. 362.*

[12] Zheng, Y.J., et al., State-of-charge inconsistency estimation of lithium-ion battery pack using mean-difference model and extended Kalman filter.*Journal of Power Sources, 2018. 383: p. 50-58.*

[13] Wang, K., et al., State of Charge (SOC) Estimation of Lithium-ion Battery Based on Adaptive Square Root Unscented Kalman Filter.*International Journal of Electrochemical Science, 2020. 15(9): p. 9499-9516.*

[14] Liu, X.Y., W.L. Li, and A.G. Zhou, PNGV Equivalent Circuit Model and SOC Estimation Algorithm for Lithium Battery Pack Adopted in AGV Vehicle.*Ieee Access, 2018. 6: p. 23639-23647.*

[15] Saxena, A.R. and D. Kumar, Design and control of a reconfigurable high-gain battery integrated dc-dc boost converter for time-varying loads.*International Journal of Circuit Theory and Applications, 2020.*

[16] Feng, Y., et al., Robust Estimation for State-of-Charge and State-of-Health of Lithium-Ion Batteries Using Integral-Type Terminal Sliding-Mode Observers.*Ieee Transactions on Industrial Electronics, 2020. 67(5): p. 4013-4023.*

[17] Shen, S., et al., Deep convolutional neural networks with ensemble learning and transfer learning for capacity estimation of lithium-ion batteries. Applied. *Energy, 2020. 260.*

[18] Sun, D.M., et al., State of charge estimation forlithium-ionbattery based on an intelligent adaptive unscented Kalman filter.*International Journal of Energy Research, 2020. 44(14): p. 11199-11218.*

[19] Li, D.M., L. Gu, and L.X. Zhu, Identification and parameter estimation algorithm of radar signal subtle features.*Physical Communication, 2020. 42.*

[20] Huang, K., K. An, and G.H.D. Correia, Planning station capacity and fleet size of one-way electric carsharing systems with continuous state of charge functions.*European Journal of Operational Research, 2020. 287(3): p. 1075-1091.*

[21] Ji, Y.J., S.L. Qiu, and G. Li, Simulation of second-order RC equivalent circuit model of lithium battery based on variable resistance and capacitance.*Journal of Central South University, 2020. 27(9): p. 2606-2613.*
[22] Chiang, Y.H., W.Y. Sean, and J.C. Ke, Online estimation of internal resistance and open-circuit voltage of lithium-ion batteries in electric vehicles.*Journal of Power Sources, 2011. 196(8): p. 3921-3932.*
[23] Hu, T.S., B. Zanchi, and J.P. Zhao, Simple Analytical Method for Determining Parameters of Discharging Batteries.*Ieee Transactions on Energy Conversion, 2011. 26(3): p. 787-798.*
[24] Mei, W.N., et al., An investigation on expansion behavior of lithium ion battery based on the thermal-mechanical coupling model.*Journal of Cleaner Production, 2020. 274.*
[25] Ouyang, Q., et al., Adaptive Square-Root Unscented Kalman Filter-Based State-of-Charge Estimation for Lithium-Ion Batteries with Model Parameter Online Identification.*Energies, 2020. 13(18).*
[26] Li, S.E., et al., Kalman filter-based tracking of moving objects using linear ultrasonic sensor array for road vehicles.*Mechanical Systems and Signal Processing, 2018. 98: p. 173-189.*
[27] Shuai, W.Q., E.Y. Li, and H. Wang, An equivalent circuit model of a deformed Li-ion battery with parameter identification.*International Journal of Energy Research, 2020. 44(11): p. 8372-8387.*
[28] How, D.N.T., et al., State of Charge Estimation for Lithium-Ion Batteries Using Model-Based and Data-Driven Methods: A Review.*Ieee Access, 2019. 7: p. 136116-136136.*
[29] Yang, J.F., et al., Online state-of-health estimation for lithium-ion batteries using constant-voltage charging current analysis.*Applied Energy, 2018. 212: p. 1589-1600.*
[30] Li, W.L., et al., State of Charge Estimation of Lithium-Ion Batteries Using a Discrete-Time Nonlinear Observer.*Ieee Transactions on Industrial Electronics, 2017. 64(11): p. 8557-8565.*
[31] Zhao, T.Z., et al., A study on half-cell equivalent circuit model of lithium-ion battery based on reference electrode.*International Journal of Energy Research, 2020.*
[32] Xiong, R., et al., A novel method to obtain the open circuit voltage for the state of charge of lithium ion batteries in electric vehicles by using H infinity filter.*Applied Energy, 2017. 207: p. 346-353.*
[33] Koseoglou, M., et al., Highly Effective Cell Equalization in a Lithium-Ion Battery Management System.*Ieee Transactions on Power Electronics, 2020. 35(2): p. 2088-2099.*
[34] Ning, X.Z., Z. Wang, and B. Wu, Kalman Filter-Based Adaptive Delay Compensation for Benchmark Problem in Real-Time Hybrid Simulation.*Applied Sciences-Basel, 2020. 10(20).*
[35] Peng, N., et al., Online parameters identification and state of charge estimation for lithium-ion batteries using improved adaptive dual unscented Kalman filter.*International Journal of Energy Research, 2020.*
[36] Jerouschek, D., et al., Data Preparation and Training Methodology for Modeling Lithium-Ion Batteries Using a Long Short-Term Memory Neural Network for Mild-Hybrid Vehicle Applications.*Applied Sciences-Basel, 2020. 10(21).*
[37] Wang, Q.K., et al., Design and management of lithium-ion batteries: *A perspective from modeling, simulation, and optimization. Chinese Physics B, 2020. 29(6).*
[38] Pang, H., L.J. Mou, and L. Guo, Parameter identification and state-of-charge estimation approach for enhanced lithium-ion battery equivalent circuit model considering influence of ambient temperatures.*Chinese Physics B, 2019. 28(10).*
[39] Cui, X.Y., et al., A New Method for State of Charge Estimation of Lithium-Ion Batteries Using Square Root Cubature Kalman Filter.*Energies, 2018. 11(1).*
[40] Ting, T.O., et al., Tuning of Kalman Filter Parameters via Genetic Algorithm for State-of-Charge Estimation in Battery Management System.*Scientific World Journal, 2014.*
[41] Jiang, L., et al., Hybrid charging strategy with adaptive current control of lithium-ion battery for electric vehicles.*Renewable Energy, 2020. 160: p. 1385-1395.*
[42] Tan, C.M., P. Singh, and C. Chen, Accurate Real Time On-Line Estimation of State-of-Health and Remaining Useful Life of Li ion Batteries.*Applied Sciences-Basel, 2020. 10(21).*
[43] Li, L., et al., State of Charge Estimation for Lithium-Ion Power Battery Based on H-Infinity Filter Algorithm.*Applied Sciences-Basel, 2020. 10(18).*
[44] Afshar, S., K. Morris, and A. Khajepour, State-of-Charge Estimation Using an EKF-Based Adaptive Observer.*Ieee Transactions on Control Systems Technology, 2019. 27(5): p. 1907-1923.*
[45] Xie, J.L., et al., Estimating the State-of-Charge of Lithium-Ion Batteries Using an H-Infinity Observer with Consideration of the Hysteresis Characteristic.*Journal of Power Electronics, 2016. 16(2): p. 643-653.*

[46] Nikohan, A., et al., Complete cell-level lithium-ion electrical ECM model for different chemistries (NMC, LFP, LTO) and temperatures (-5 degrees C to 45 degrees C) - Optimized modelling techniques.*International Journal of Electrical Power & Energy Systems, 2018. 98: p. 133-146.*

[47] Soltani, M., et al., Parameters identification and discharge capacity prediction of Nickel-Metal Hydride battery based on modified fuzzy c-regression models. *Neural Computing & Applications, 2020.* ***32****(15): p. 11361-11371.*